Huygens Subgridding for the Frequency-Dependent–Finite-Difference Time-Domain Method

Maksims Abaļenkovs

Microwave and Communication Systems Group
School of Electrical and Electronic Engineering
The University of Manchester

Informal Numerical Analysis Seminar

Outline

1. Introduction
2. Finite-Difference Time-Domain (FDTD)
3. Frequency-Dependent–Finite-Difference Time-Domain (FD–FDTD)
4. Subgridding
5. Total-Field/Scattered-Field Technique
6. Huygens Subgridding
7. Frequency-Dispersive Huygens Subgridding
8. Numerical Results
9. Conclusion
10. Future Work

Motivation

- object simulation on a computer → prototype
- objects grow in size and geometric complexity
- need to simulate frequency-dispersive materials
- Finite-Difference Time-Domain (FDTD) method's popularity

Problems

- interdependence of the spatial and temporal discretisation steps
- Courant–Friedrichs–Lewy (CFL) stability condition
- fine geometric features → high spatio-temporal resolution
- high resolution → computationally expensive

Solutions

- subgridding to increase the FDTD efficiency
- simulation domain: several subdomains with different resolution
- main grid (coarse resolution): homogeneous object parts
- subgrid (fine resolution): delicate features of an object
- the CFL condition: maintained separately in each grid
- promising subgridding technique: Huygens Subgridding (HSG)

Contributions

- extension of dispersive HSG method 1D $\rightarrow$ 3D
- implementation of 3D method in Fortran 90
- setting of radio environment from PGM files
- simulation of wave propagation from defibrillator pads
- analysis of computational requirements

Maxwell's Equations in Three Dimensions

Faraday's law:

$$\frac{\partial \boldsymbol{B}}{\partial t} = -\nabla \times \boldsymbol{E} - \boldsymbol{M}, \tag{1}$$

Ampère's law:

$$\frac{\partial \boldsymbol{D}}{\partial t} = \quad \nabla \times \boldsymbol{H} - \boldsymbol{J}, \tag{2}$$

Gauss' law for electric field:

$$\nabla \cdot \boldsymbol{D} = 0, \tag{3}$$

Gauss' law for magnetic field:

$$\nabla \cdot \boldsymbol{B} = 0. \tag{4}$$

MANCHESTER 1824
The University of Manchester

Maxwell's curl equations

For linear, isotropic, non-dispersive and lossy materials:

$$\frac{\partial \boldsymbol{H}}{\partial t} = -\frac{1}{\mu}\nabla \times \boldsymbol{E} - \frac{1}{\mu}\left(\boldsymbol{M}_{src} + \sigma^{*}\boldsymbol{H}\right), \tag{5}$$

$$\frac{\partial \boldsymbol{E}}{\partial t} = \frac{1}{\varepsilon}\nabla \times \boldsymbol{H} - \frac{1}{\varepsilon}\left(\boldsymbol{J}_{src} + \sigma\boldsymbol{E}\right). \tag{6}$$

Foundation of the FDTD method, magnetic field

$$\frac{\partial H_x}{\partial t} = \frac{1}{\mu}\left[\frac{\partial E_y}{\partial z} - \frac{\partial E_z}{\partial y} - (M_{src,x} + \sigma^* H_x)\right], \tag{7}$$

$$\frac{\partial H_y}{\partial t} = \frac{1}{\mu}\left[\frac{\partial E_z}{\partial x} - \frac{\partial E_x}{\partial z} - (M_{src,y} + \sigma^* H_y)\right], \tag{8}$$

$$\frac{\partial H_z}{\partial t} = \frac{1}{\mu}\left[\frac{\partial E_x}{\partial y} - \frac{\partial E_y}{\partial x} - (M_{src,z} + \sigma^* H_z)\right]. \tag{9}$$

Foundation of the FDTD method, electric field

$$\frac{\partial E_x}{\partial t} = \frac{1}{\varepsilon}\left[\frac{\partial H_z}{\partial y} - \frac{\partial H_y}{\partial z} - (J_{src,x} + \sigma E_x)\right], \tag{10}$$

$$\frac{\partial E_y}{\partial t} = \frac{1}{\varepsilon}\left[\frac{\partial H_x}{\partial z} - \frac{\partial H_z}{\partial x} - (J_{src,y} + \sigma E_y)\right], \tag{11}$$

$$\frac{\partial E_z}{\partial t} = \frac{1}{\varepsilon}\left[\frac{\partial H_y}{\partial x} - \frac{\partial H_x}{\partial y} - (J_{src,z} + \sigma E_z)\right]. \tag{12}$$

Placement of the field components in space

- Electric field components: in the middle of the cell faces.
- Magnetic field components: in the middle of the cell edges.

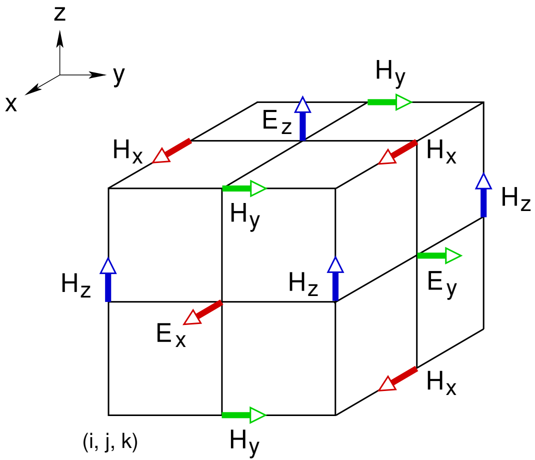

Figure: Yee unit cell [1]

Placement of the field components in time

- Half time-step offset makes the FDTD method explicit
- E^n depends on E^{n-1} and $H^{n-1/2}$

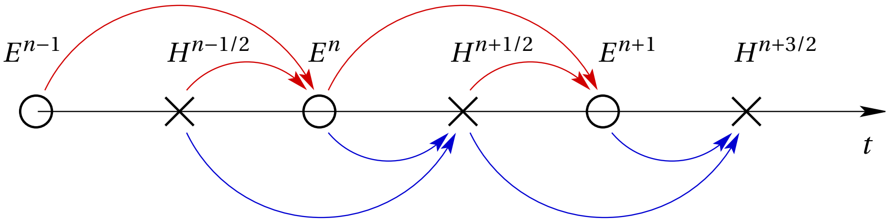

Figure: Placement of the leap-frog components in time [2]

Central-difference approximations

Space derivative:

$$\frac{\partial u}{\partial x}\left(i\Delta x, j\Delta y, k\Delta z, n\Delta t\right) = \frac{u^n\left(i+\frac{1}{2}, j, k\right) - u^n\left(i-\frac{1}{2}, j, k\right)}{\Delta x} + O\left((\Delta x)^2\right), \quad (13)$$

Time derivative:

$$\frac{\partial u}{\partial t}\left(i\Delta x, j\Delta y, k\Delta z, n\Delta t\right) = \frac{u^{n+\frac{1}{2}}\left(i, j, k\right) - u^{n-\frac{1}{2}}\left(i, j, k\right)}{\Delta t} + O\left((\Delta t)^2\right), \quad (14)$$

Semi-implicit approximation:

$$u^n\left(i, j, k\right) = \frac{u^{n+\frac{1}{2}}\left(i, j, k\right) + u^{n-\frac{1}{2}}\left(i, j, k\right)}{2}. \quad (15)$$

Causes of frequency dispersion

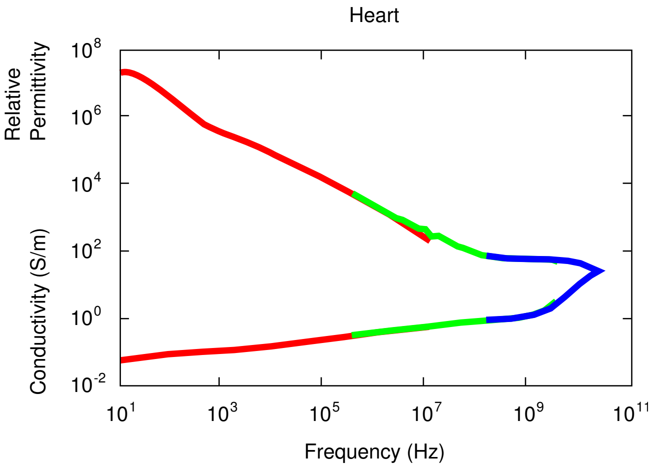

Figure: Experimental data measured in the frequency region of 10 Hz to 20 GHz. Colours denote the low, medium, high frequency regimes [3].

Models for frequency dispersion

Debye relaxation:

$$\varepsilon_r(\omega) = \varepsilon_\infty + \sum_{p=1}^{P} \frac{\Delta\varepsilon_p}{1 + \jmath\omega\tau_p}, \tag{16}$$

Lorentz–Drude:

$$\varepsilon_r(\omega) = \varepsilon_\infty + \sum_{p=1}^{P} \frac{\Delta\varepsilon_p \omega_p^2}{\omega_p^2 + 2\jmath\omega\delta_p - \omega_p^2}, \tag{17}$$

Drude:

$$\varepsilon_r(\omega) = \varepsilon_\infty - \sum_{p=1}^{P} \frac{\omega_p^2}{\omega^2 - \jmath\omega\tau_p^{-1}}, \tag{18}$$

Cole–Cole:

$$\varepsilon_r(\omega) = \varepsilon_\infty + \sum_{p=1}^{P} \frac{\Delta\varepsilon_p}{1 + (\jmath\omega\tau_p)^\alpha}. \tag{19}$$

Auxiliary Differential Equation (ADE) method

$$\frac{\partial \boldsymbol{D}}{\partial t} = \nabla \times \boldsymbol{H}, \tag{20}$$

$$\boldsymbol{D} = \varepsilon \boldsymbol{E} = \varepsilon_0 \varepsilon_r \boldsymbol{E} = \varepsilon_0 \left(\varepsilon_\infty + \frac{\sigma}{\jmath \omega \varepsilon_0} + \frac{\varepsilon_s - \varepsilon_\infty}{1 + \jmath \omega \tau} \right) \boldsymbol{E}, \tag{21}$$

$$\jmath^2 \omega^2 \tau \boldsymbol{D} + \jmath \omega \boldsymbol{D} = \jmath^2 \omega^2 \tau \varepsilon_0 \varepsilon_\infty \boldsymbol{E} + \jmath \omega (\sigma \tau + \varepsilon_0 \varepsilon_s) \boldsymbol{E} + \sigma \boldsymbol{E}, \tag{22}$$

$$\frac{\partial^2 (\tau \boldsymbol{D})}{\partial t^2} + \frac{\partial \boldsymbol{D}}{\partial t} = \frac{\partial^2 (\tau \varepsilon_0 \varepsilon_\infty \boldsymbol{E})}{\partial t^2} + \frac{\partial ((\sigma \tau + \varepsilon_0 \varepsilon_\infty) \boldsymbol{E})}{\partial t} + \sigma \boldsymbol{E}. \tag{23}$$

Auxiliary Differential Equation for the electric field

$$E^{n+\frac{1}{2}} = C_1 D^{n+\frac{1}{2}} - C_2 D^{n-\frac{1}{2}} + C_3 D^{n-\frac{3}{2}} + C_4 E^{n-\frac{1}{2}} - C_5 E^{n-\frac{3}{2}}, \tag{24}$$

where

$$C_1 = \frac{\tau + \Delta t}{\varphi}, \quad C_2 = \frac{2\tau + \Delta t}{\varphi}, \quad C_3 = \frac{\tau}{\varphi}, \quad C_4 = \frac{\chi}{\varphi}, \quad C_5 = \frac{\alpha}{\varphi}$$

with

$$\alpha = \varepsilon_0 \varepsilon_\infty \tau, \quad \beta = \varepsilon_0 \varepsilon_s + \sigma\tau, \quad \varphi = \alpha + \Delta t \beta + \frac{\Delta t^2 \sigma}{2}, \quad \chi = 2\alpha + \Delta t \beta - \frac{\Delta t^2 \sigma}{2}.$$

Aim of subgridding

Increase of simulation efficiency

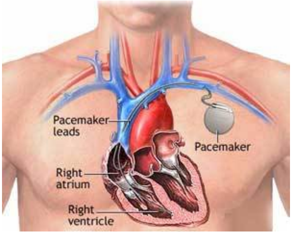

(a) Pacemaker[1]

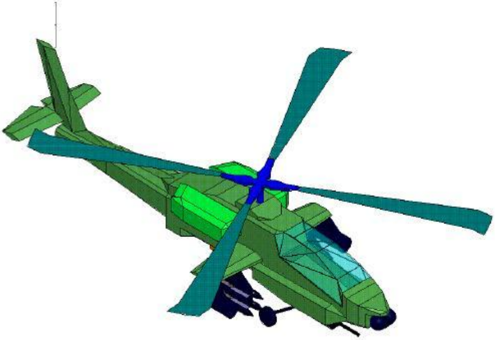

(b) Helicopter[2]

[1] Amazing Data, 19 Unintentional Discoveries that Changed the World, http://amazingdata.com/19-unintentional-discoveries-that-changed-the-world/

[2] ANSYS, Antenna Co-Site Simulation, 2009, http://www.ansoft.co.kr/html/eve_tra/infoday/06AntennaCo-SiteSimulation.pdf

Key aspects of subgridding

- subgridding interface
- subgridding ratio $r = \frac{\Delta s_a}{\Delta s_b} = \frac{\Delta t_a}{\Delta t_b}$
- time advancement
- grid geometry
- grid recursion
- number of subgrids
- stability
- accuracy
- adaptability
- material traverse
- performance cost
- parallelisation

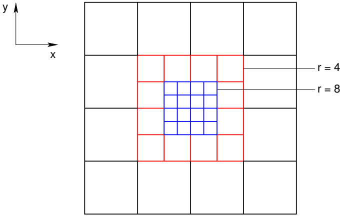

(a) Grid recursion

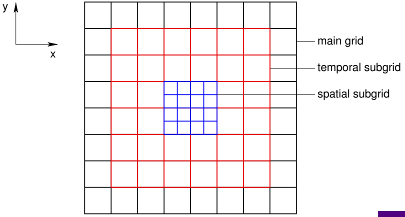

(b) Interface decoupling

Total-Field/Scattered-Field zoning

$$E_{tot} = E_{inc} + E_{sct}, \quad H_{tot} = H_{inc} + H_{sct} \tag{25}$$

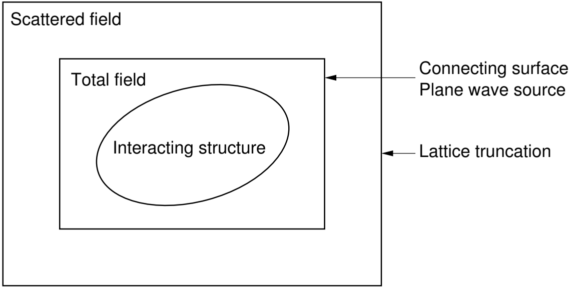

- incident-wave fields: known at all spatio-temporal nodes
- scattered-wave fields: unknown, incident wave $\leftrightarrow$ materials [1]

MANCHESTER 1824 The University of Manchester

Total-Field/Scattered-Field component locations, 1D

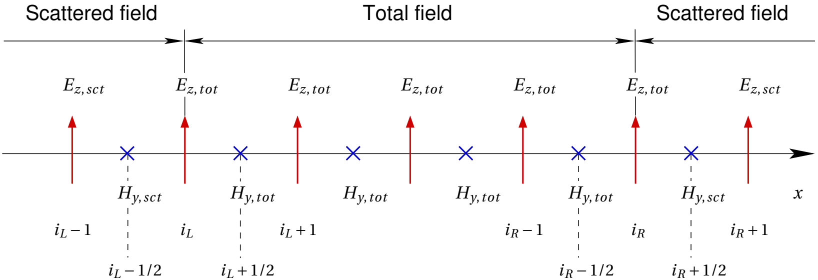

$$E_{z,tot}^{n+1}(i_L) = E_{z,tot}^{n}(i_L) + \frac{\Delta t}{\varepsilon_0 \Delta x}\left(H_{y,tot}^{n+\frac{1}{2}}\left(i_L + \tfrac{1}{2}\right) - H_{y,sct}^{n+\frac{1}{2}}\left(i_L - \tfrac{1}{2}\right)\right),$$

$$E_{z,tot}^{n+1}(i_L) = E_{z,tot}^{n}(i_L) + \frac{\Delta t}{\varepsilon_0 \Delta x}\left(H_{y,tot}^{n+\frac{1}{2}}\left(i_L + \tfrac{1}{2}\right) - H_{y,sct}^{n+\frac{1}{2}}\left(i_L - \tfrac{1}{2}\right) - H_{y,inc}^{n+\frac{1}{2}}\left(i_L - \tfrac{1}{2}\right)\right).$$

HSG, Introduction

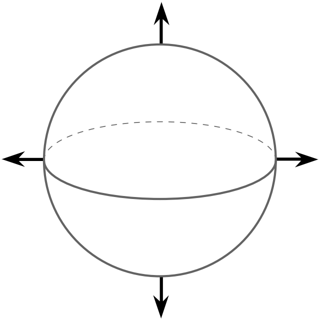

- no direct connection between grids
- influence: equivalent currents via Huygens Surfaces
- low reflection from the interface
- unlimited subgridding ratio
- suffers from instability

Huygens surface radiation

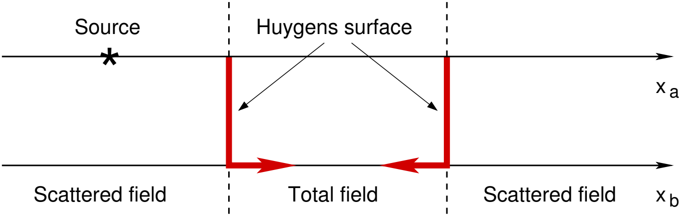

(a) Radiation from main to subgrid

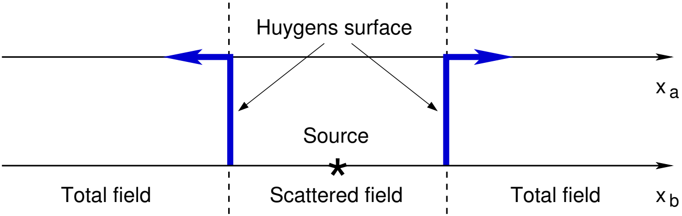

(b) Radiation from subgrid to main grid

HSG domain decomposition, 2D

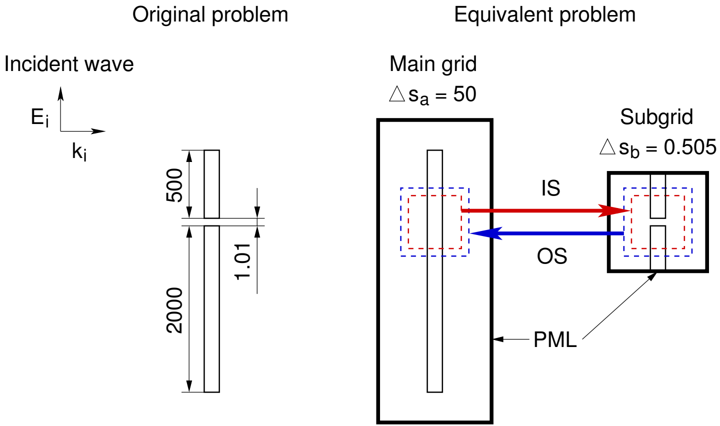

Figure: Subgridding ratio $r = 99$ [4].

Inner Surface, 1D

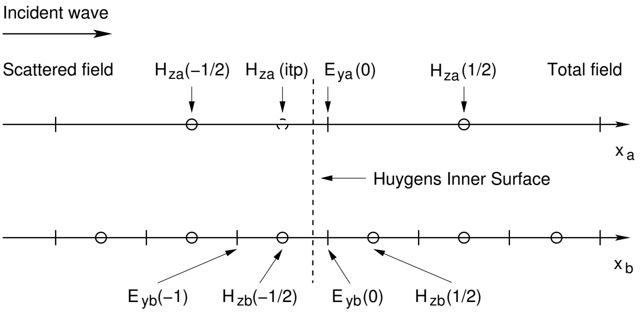

$$E_{yb}^{n+m}(0) = E_{yb}^{n+m-1}(0) - \frac{\Delta t_b}{\varepsilon_0 \Delta x_b}\left(H_{zb}^{n+m-\frac{1}{2}}\left(\tfrac{1}{2}\right) - H_{zb}^{n+m-\frac{1}{2}}\left(-\tfrac{1}{2}\right) - H_{za}^{n+m-\frac{1}{2}}(itp)\right)$$

Outer Surface, 1D

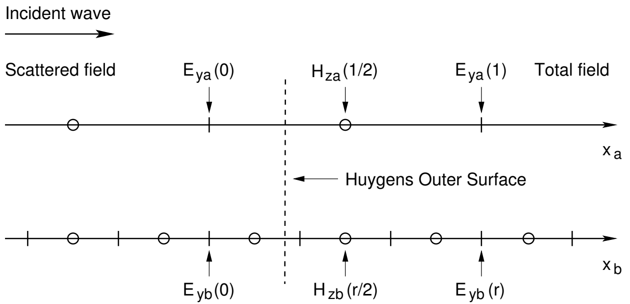

$$E_{ya}^{n+r}(0) = E_{ya}^{n}(0) - \frac{\Delta t_a}{\varepsilon_0 \Delta x_a}\left(H_{za}^{n+\frac{r}{2}}\left(\tfrac{1}{2}\right) - H_{za}^{n+\frac{r}{2}}\left(-\tfrac{1}{2}\right) - H_{zb}^{n+\frac{r}{2}}\left(\tfrac{r}{2}\right)\right)$$

HSG advancement on time

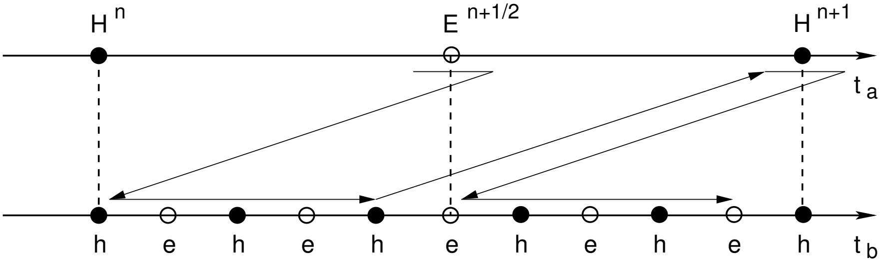

Filtering in HSG

$$E_a(ia1) = \frac{1}{4}E_a(ia1-1) + \frac{1}{2}E_a(ia1) + \frac{1}{4}E_a(ia1+1), \tag{26}$$

$$H_a(itp) = \frac{1}{4}H_a(itp-2) + \frac{1}{2}H_a(itp-1) + \frac{1}{4}H_a(itp). \tag{27}$$

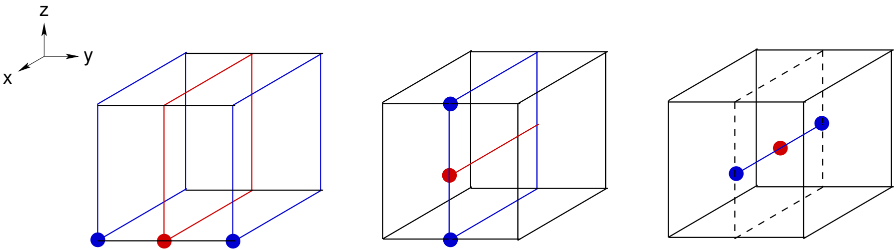

HS with electric flux density and magnetic field, 1D

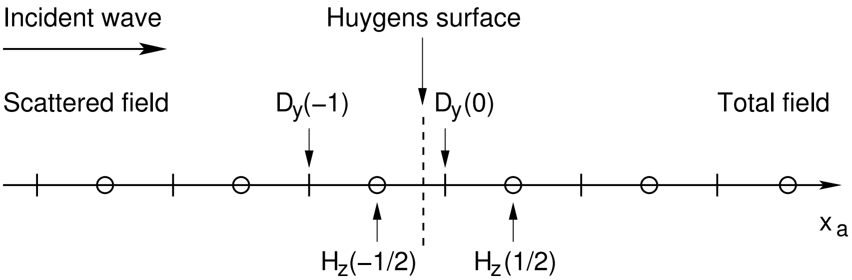

$$D_y^{n+1}(0) = D_y^n(0) - \frac{\Delta t}{\Delta x}\left(H_{z,tot}^{n+\frac{1}{2}}\left(\tfrac{1}{2}\right) - H_{z,sct}^{n+\frac{1}{2}}\left(-\tfrac{1}{2}\right) - H_{z,inc}^{n+\frac{1}{2}}\left(-\tfrac{1}{2}\right)\right) \tag{28}$$

Simulation settings

Parameter	HSG	Fine
ni, nj, nk	$1 \sim 80$	$1 \sim 400$
t_{max}	2000	10000
r	5	
n_{pml_a}	10	
n_{pml_b}	6	
source type	soft	soft
Δs_a	10 mm	–
Δs_b	2 mm	2 mm
Δt_a	0.179 ps	–
Δt_b	3.582 ps	3.582 ps
N_{CFL}	0.93	0.93
χ_a	5	–
χ_b	25	25

Excitation waveform

Gaussian pulse

$$J_z^t = \exp\left[-\left(\frac{t-3T}{T}\right)^2\right],$$

where

$$T = \frac{1}{2f_{max}}, \quad f_{max} = 6 \cdot 10^9 \text{ Hz}.$$

Gaussian pulse, time domain

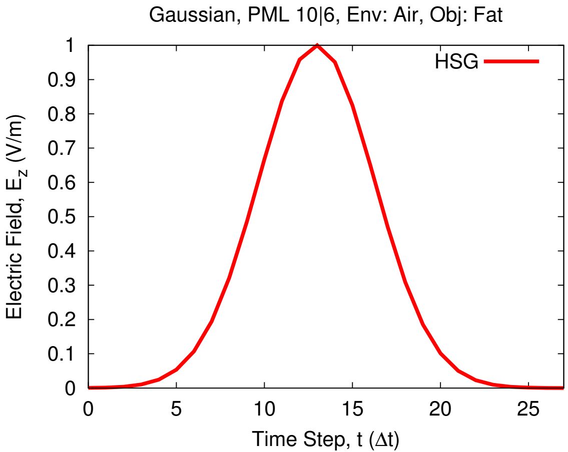

Gaussian pulse, frequency domain

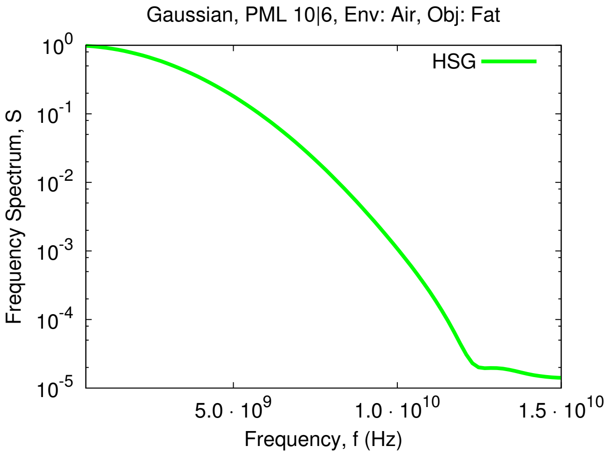

Debye relaxation, media parameters

Medium	σ [S/m]	ε_s	ε_∞	τ [ps]
Air	0.00	1.00	1.00	0.00
Fat	0.04	5.53	4.00	0.24
Heart	1.02	63.55	34.91	0.29
Bone	0.10	14.17	7.36	0.34
Muscle	0.75	56.93	28.00	0.19

Scenario 1. Air

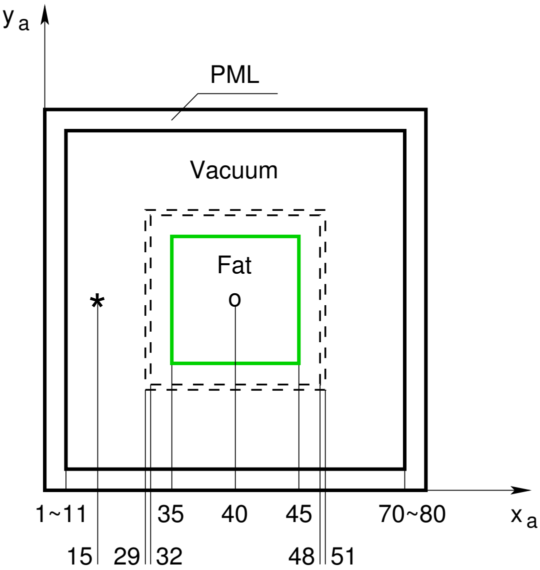

Scenario 1a, time domain

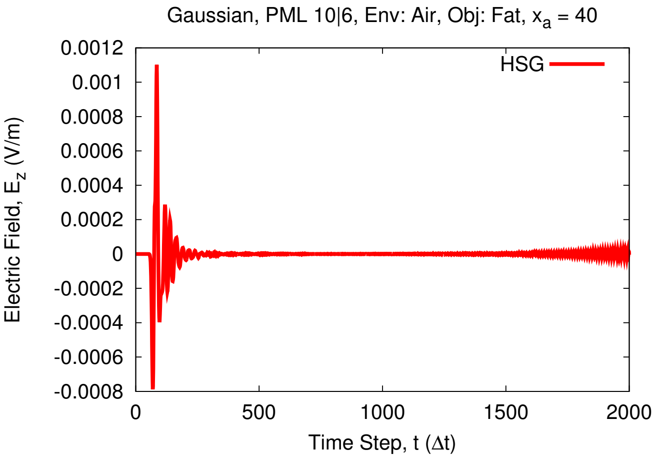

Scenario 1b, time domain

Excitation source in Fat in the subgrid delays the HSG instability.

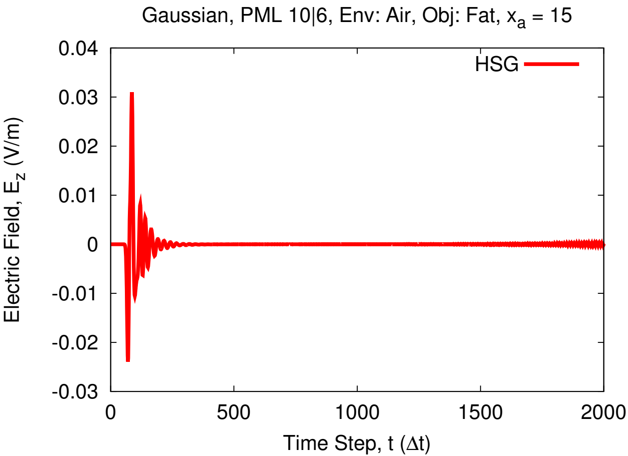

Scenario 4. Multiple inhomogeneous weak and strong media

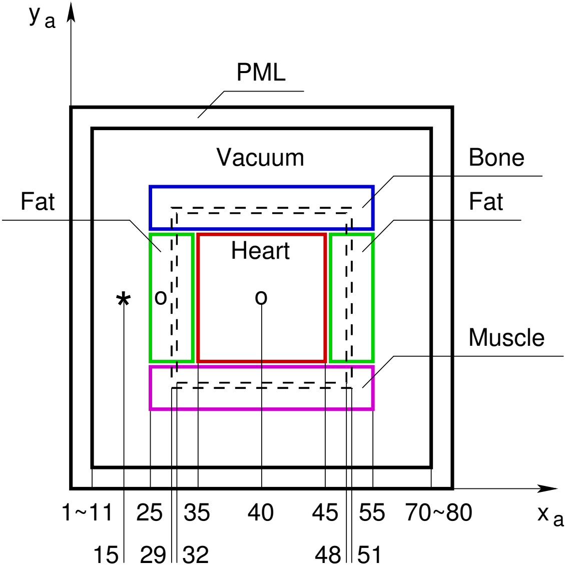

Scenario 4, time domain

- Strong Debye in the Inner Box reduces the signal amplitudes.
- High resolution of the subgrid: good agreement with the fine grid.

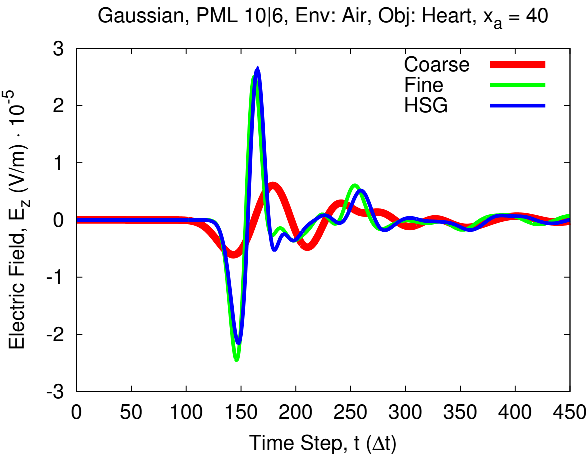

Scenario 4, frequency domain

- High resolution subgrid of the HSG ⇒
- Almost identical performance to the fine grid signal.

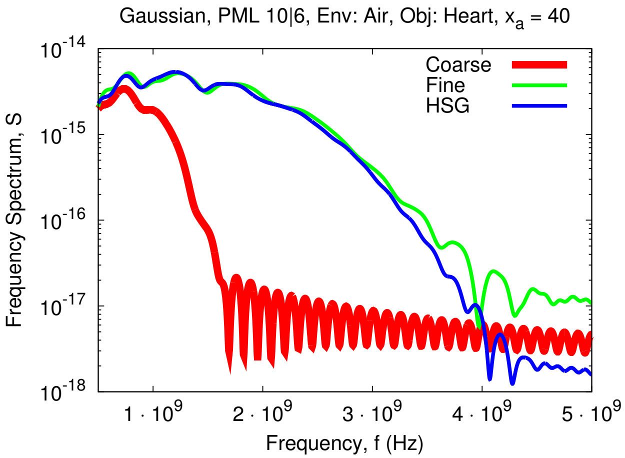

Scenario 5. HSG stability in the homogeneous weak medium

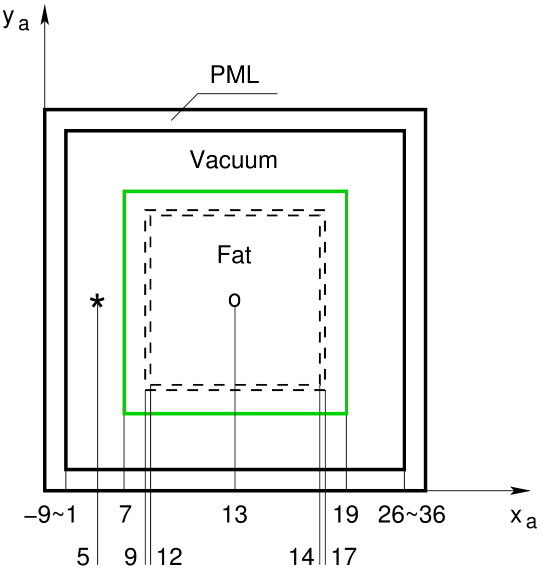

Scenario 5, time domain

- Cases plotted: $\sigma = 0$ and $\sigma = 3.71 \cdot 10^n$, where $n \in [-2, 0, 2]$.
- $\sigma = 0$: divergence after $\approx 170\,000$ time-steps.

The University of Manchester

Simulation of defibrillation

- Research of defibrillators → defibrillation success rate ↑
- Successful defibrillation, factors:
  - current level
  - defibrillator waveform
  - electrode size, shape and position
  - transthoracic impedance

Simulation settings, human torso

Parameter	HSG	Fine
ni	$-13 \sim 67$	$-53 \sim 319$
nj	$-3 \sim 102$	$-3 \sim 494$
nk	$160 \sim 341$	$820 \sim 1691$
t_{max}	1000	5000
r	5	
n_{pml_a}	4	
n_{pml_b}	6	
source type	soft	soft
Δs_a	5 mm	–
Δs_b	1 mm	1 mm
Δt_a	8.955 ps	–
Δt_b	1.791 ps	1.791 ps
N_{CFL}	0.93	0.93
χ_a	10	–
χ_b	50	50

MANCHESTER 1824 The University of Manchester

Human torso, scenario setting, 2D

- Human torso in the main grid with heart in the subgrid.
- Outer Surface (blue) and Inner Surface (red) bound the subgrid region.

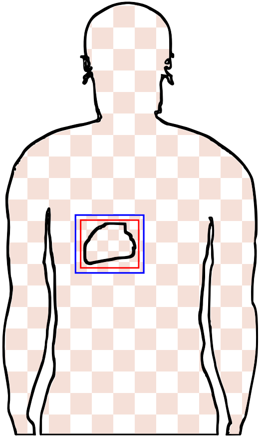

Human torso, scenario setting, 3D

Heart (red) and two defibrillator pads (green, purple) placed anteroposteriorly.

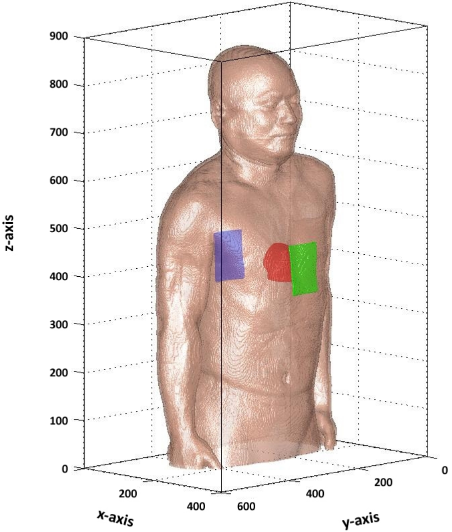

Scenario setting, 1D as viewed by the main grid of the HSG

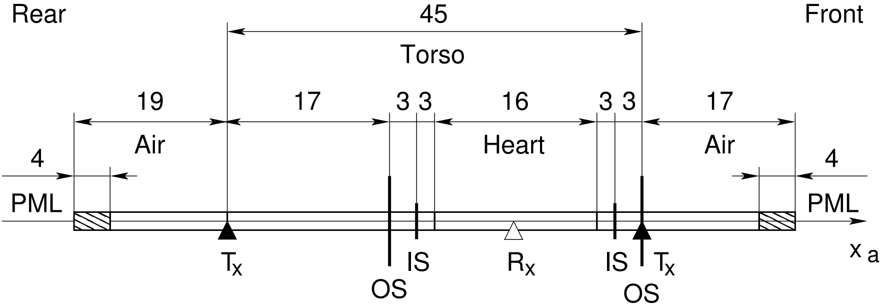

- Observation point R_x is in the middle of the heart.
- Rectangular pads T_x, where present, coincide with skin.
- Numerical values are given in the main grid units.

Human torso, time domain

Strong initial signal from the pad allows to preserve high signal amplitudes.

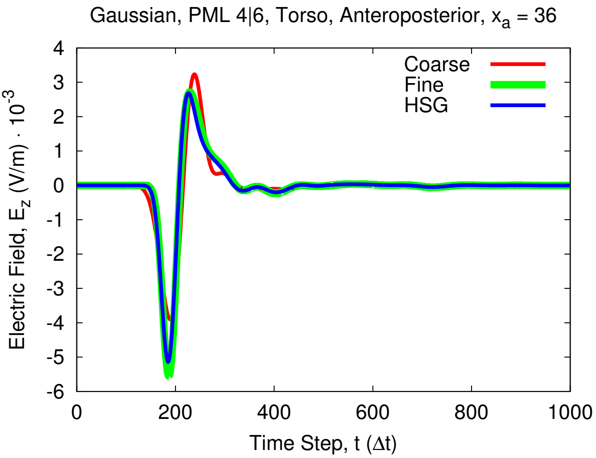

MANCHESTER 1824
The University of Manchester

Human torso, frequency domain

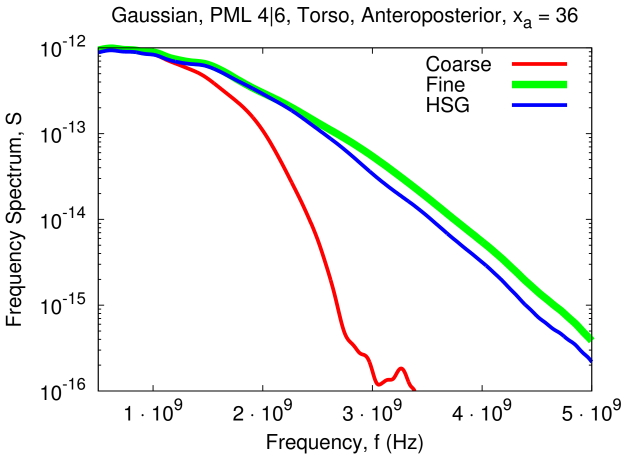

HSG memory consumption relative to the all fine grid case

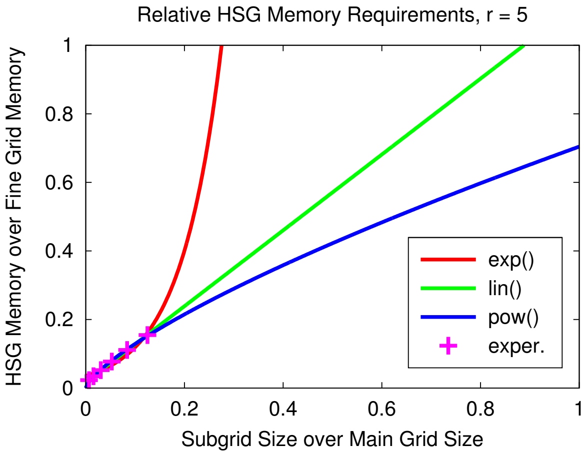

HSG time consumption relative to the all fine grid case

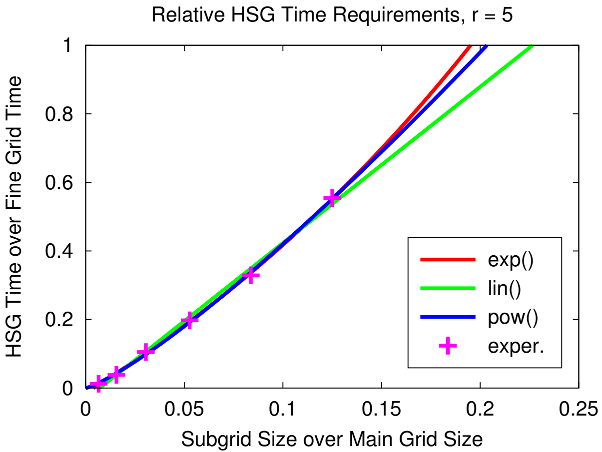

Conclusion

Major:

- adaptation of the promising Huygens Subgridding (HSG)
- main contribution: dispersive HSG method 1D → 3D
- efficient simulation of the frequency-dispersive materials
- Auxiliary Differential Equation (ADE)
- one-pole Debye relaxation model

Minor:

- radio environment setting: PGM files
- application test case: wave propagation from the defibrillator pads
- analysis of the computational requirements, dispersive HSG ($r = 5$)
- dispersive HSG ($r = 5$) vs. the all fine grid FDTD: (SG $\leq$ 20% MG)

Future work

- Stability
  - decoupling of spatial and temporal interfaces
  - implicit FDTD scheme in the subgrid region
- Defibrillation
  - defibrillation current density and current flow distribution in the heart
  - implementation of realistic defibrillator waveforms
  - Thin Slab method: main grid cells larger than the medium size
- Efficiency
  - parallelisation: MPI, CUDA, Chapel

Bibliography

- Allen Taflove, Susan C. Hagness
  Computational Electrodynamics:
  The Finite-Difference Time-Domain Method, 3rd Edition
  Artech House, 2005

- Andrew F. Peterson, Scott L. Ray, Raj Mittra
  Computational Methods for Electromagnetics
  IEEE Press, Oxford University Press, 1998

- Camelia Gabriel, Sami Gabriel
  Compilation of the Dielectric Properties of Body Tissues at RF and Microwave Frequencies
  Physics Dept., King's College London, 1996

- Jean-Pierre Bérenger
  A FDTD Subgridding Based on Huygens Surfaces
  IEEE AP-S International Symposium,
  2005, Washington D.C.

Discussion:

- thank you for attention
- questions and answers.

The University of Manchester